Journal of
Materials Chemistry C

PAPER

View Article Online
View Journal | View Issue

Cite this: *J. Mater. Chem. C*, 2016, **4**, 10453

[{$VOCl_2(CH_2(COOEt)_2)$}$_4$] as a molecular precursor for thermochromic monoclinic VO_2 thin films and nanoparticles†

Ben Blackburn, Michael J. Powell, Caroline E. Knapp, Joseph C. Bear,* Claire J. Carmalt and Ivan P. Parkin

Received 12th August 2016,
Accepted 19th October 2016

DOI: 10.1039/c6tc03482a

www.rsc.org/MaterialsC

The synthesis of thermochromic monoclinic vanadium(IV) oxide (VO_2 (M)) thin films and vanadium oxide nanocrystals from a molecular precursor, [{$VOCl_2(CH_2(COOEt)_2)$}$_4$] is described. Thin films were synthesised using aerosol assisted chemical vapour deposition (AACVD) onto glass substrates at high temperatures and were subsequently characterised and tested for thermochromic efficiency. The film's suitability as smart, energy efficient window coatings was investigated by calculating their solar modulation potential. Thin films were also doped with tungsten to lower their metal to semiconductor transition temperature (MST) through the addition of tungsten(VI) phenoxide during the AACVD process, lowering the MST from a typical ~70 °C for an undoped VO_2 (M) thin film to ~50 °C for a typical W-doped example. The optimum deposition temperature of 550 °C produced films with thermochromic properties (solar modulation of 15.9%) comparable to the highest values reported. In addition, vanadium oxide nanostructures were synthesised using the thermal decomposition of [{$VOCl_2(CH_2(COOEt)_2)$}$_4$] and their shape controllably tailored by varying surfactant concentration and type. Thin films and nanostructures were characterised using X-ray diffraction (XRD), scanning electron microscopy (SEM), transmission electron microscopy (TEM), X-ray photoelectron spectroscopy (XPS) and energy-dispersive X-ray spectroscopy (EDS). Thermochromic measurements were measured using UV-Vis spectroscopy with a variable temperature stage.

Introduction

The synthesis of monoclinic vanadium dioxide thin films and nanocrystals for energy saving, infrared radiation reflecting windows is currently an area of intense research due in no small part to the ever-increasing pressure placed on world energy feedstocks.[1–4] Therefore the need to reduce energy consumption or switch to sustainable energy sources have never been greater. Buildings contribute approximately 1/3 of greenhouse gas emissions, with the majority of these being due to heating and cooling loads to maintain a narrow range of temperatures.[5] The employment of smart, energy saving materials such as thermochromic VO_2 window coatings is one such initiative to moderate this vast energy consumption.

The monoclinic phase vanadium(IV) oxide (VO_2 (M)) undergoes a structural transition to the rutile phase (VO_2 (R)) at a metal to semiconductor transition temperature (MST) of *ca.* 68 °C, a phenomenon known as thermochromism.[6,7] VO_2 (M) is of particular interest as its MST is relatively close to that of room temperature, unlike other thermochromic V_xO_y species, such as V_2O_3.[8] Below the MST, VO_2 (M) is a semiconductor that transmits infrared and ultraviolet radiation consistently, whereas above the MST, VO_2 (R) exhibits metallic conduction, reflecting in the same region.[1,9] This property is crucial in the design of smart window coatings, that are transmissive of near IR wavelengths at low temperatures, but reflective at high temperatures, thus alleviating the use of expensive and energy-intensive air conditioning units in hot countries.[10] In order to decrease the MST, it is common to incorporate dopant atoms into the VO_2 matrix. Tungsten is by far the most common and most effective dopant in lowering the MST, and has the added advantage of giving the VO_2 a more aesthetically acceptable blue tint rather than the dirty yellow of VO_2 (M).[11] Other dopants such as: niobium,[12] fluorine,[13] magnesium[14] and molybdenum[15] have also been shown to reduce the MST.

The tungsten dopant in W–VO_2 has tetragonal symmetry, which distorts the monoclinic VO_2 towards the tetragonal form. Atoms with large atomic radii such as tungsten introduces distortions into the VO_2 lattice around the W centre,[16] as well as introducing areas of greater electron density into the antibonding

Department of Chemistry, University College London, 20 Gordon Street, London, WC1H 0AJ, UK. E-mail: joseph.bear.11@ucl.ac.uk

† Electronic supplementary information (ESI) available. See DOI: 10.1039/c6tc03482a

orbitals of the V–V bond, and so destabilising the monoclinic phase.[17] These factors are thought to lower the energy barrier to the MST.

The synthesis of VO_2 (M) is exacting due to the large number of stable oxide polymorphs of vanadium.[8,18] Vanadium oxides will easily form as both phase pure oxides (V_2O_3, VO_2 and V_2O_5) and mixed oxidation states (V_2O_7, V_3O_7 *etc.*) and thus isolating phase pure VO_2 (M) requires precise control of the partial pressure of oxygen in the process.[8] Thin films of VO_2 have been very well studied, with highly effective thermochromic VO_2 (M) and doped VO_2 (M) films deposited on a variety of substrates.[19–21] The paucity of low molecular weight, volatile precursors containing vanadium(IV) has led to the use of air-sensitive VCl_4[22,23] and stable $VO(acac)_2$[24] precursors. It is also noteworthy that VO_2 (M) thin films have been deposited using $VOCl_3$, a vanadium(V) source.[23,25,26]

Thin films of VO_2 (M) have been deposited using both atmospheric pressure chemical vapour deposition (APCVD)[27–30] and aerosol assisted chemical vapour deposition (AACVD) methods,[11,31,32] both of which are highly effective methods for coating large substrates with thin films of VO_2. The ability to tailor the vanadium precursor could lead to improved properties in the deposited films. This could be achieved by the synthesis of a single molecular precursor, which would have benefits such as the ability to precisely control dopant levels to achieve a given reduction in the phase transition temperature. To this end, AACVD is the preferred method for the CVD of single molecular precursors, due to the typical low volatility of such species.[33–35]

The majority of synthetic methods for the synthesis of nanoparticles and nanostructures have focussed on high temperature methods.[36–38] Vanadium oxide nanoparticles have been synthesised using a variety of methods, including: pyrolysis,[39] sol–gel,[40] hydrothermal methods[41] and ball milling[42] for use in coatings. Hydrothermal (autoclaving) and sol–gel methods tend to produce large, highly crystalline VO_2 (M) nanostructures, from vanadium precursors in the presence of reducing agents such as acids to prevent over-oxidation to V_2O_5.[37,43,44] Autoclave methods have also shown to be effective in the growth of large nanowires, and remain the most widely used bottom-up method for the synthesis of VO_2 (M) nanocrystals. It is noteworthy that the manipulation of the gaseous environment to contain partial amounts of oxygen in order to prevent the reduction/oxidation of $V^{(IV)}$ species has met with considerable success in aforementioned high temperature syntheses.[45–47]

However, to date, the use of single molecular precursors for vanadium oxide nanocrystals and thin films has been under-explored. Our work describes the synthesis of a single molecular precursor; dichloro(oxo) vanadium(IV) diethyl malonate [{$VOCl_2$-(CH_2($COOEt$)$_2$)}$_4$] [**1**] for VO_2 (Section 1), fabrication of doped and undoped VO_2 (M) thin films using AACVD (Section 2), and anisotropic vanadium oxide nanomaterials whose growth is controlled by surfactants (Section 3). Compound [**1**] has two key advantages over typical vanadium compounds used for the formation of VO_2 (M) thin films; superior solubility in preferred solvents for AACVD such as hexane, dichloromethane, chloroform, toluene *etc.* whereas compounds such as vanadyl acetylacetonate are sparingly soluble, and higher reactivity with oxygen due to the presence of volatile halide ligands. The films were doped with tungsten by adding small amounts of tungsten(VI) hexaphenoxide [$W(OPh)_6$] to the precursor solution, and a lowering of the MST observed. Vanadium oxide nanomaterials were synthesised by the thermal decomposition of [**1**] in the presence of a high boiling point solvent (1-octadecene) and structure directing surfactants (oleic acid and oleylamine). The structure of dichloro(oxo) vanadium(IV) diethyl malonate [{$VOCl_2$(CH_2($COOEt$)$_2$)}$_4$] [**1**] was determined by X-ray crystallography, elemental analysis, ^{1}H and ^{13}C {^{1}H} NMR spectroscopy. Thin films and nanostructures were characterised using X-ray diffraction (XRD), scanning electron microscopy (SEM), transmission electron microscopy (TEM), X-ray photoelectron spectroscopy (XPS) and energy-dispersive X-ray spectroscopy (EDS). Thermochromic measurements were measured using UV-Vis spectroscopy with a variable temperature stage.

Experimental

Materials

Vanadium(V) oxychloride (99%), diethyl malonate (ReagentPlus®, 99%), oleic acid (techn. grade, 90%), oleylamine (techn. grade, 70%), 1-octadecene (techn. grade, 90%) (dried over sodium) and 1,2-tetradecanediol (techn. grade, 90%) were purchased from Sigma Aldrich Ltd and used as received. Laboratory solvents were purchased from Sigma Aldrich Ltd and of analytical grade. Solvents were dried over activated alumina *via* the Grubbs method using anhydrous engineering equipment, ensuring that the concentration of water in the solvents was below 5–10 ppm.[48] Deuterated chloroform ($CDCl_3$) was obtained from GOSS Scientific and was degassed and dried over 3 Å molecular sieves.

Instrumentation

^{1}H and ^{13}C{^{1}H} NMR spectroscopy was carried out on a Bruker A-600 MHz spectrometer, operating at 295 K and 600.13 MHz (^{1}H). Signals are reported relative to $SiMe_4$ (δ = 0.00 ppm) and the following abbreviations are used s (singlet), d (doublet), t (triplet), q (quartet), m (multiplet), b (broad). Scanning electron microscope images were recorded on a Jeol JSM-6301F SEM at an acceleration voltage of 15 kV. Transmission electron microscopy (TEM) images and were obtained using a high resolution TEM Jeol 2100 with a LaB_6 source operating at an acceleration voltage of 200 kV. Images were recorded on a Gatan Orius Charge-coupled device (CCD). Samples were prepared by drop-casting a nanoparticle dispersion in *n*-hexane onto a 400 mesh gold grid with a thin holey carbon film (Agar Scientific). Energy dispersive X-ray spectra (EDS) were recorded on an Oxford Instruments XMax EDS detector running AZTEC software. X-Ray diffraction (XRD) patterns were recorded using a *Bruker D8 Discover* X-ray diffractometer using monochromatic Cu $K_{\alpha1}$ and Cu $K_{\alpha2}$ radiation of wavelengths 1.54056 and 1.54439 Å respectively, emitted in an intensity ratio of 2 : 1 with a voltage of 40 kV and a current of 40 mA. The incident beam angle was 1° and data was collected

between 10° and 66° 2θ with a step size of 0.05° at 2 s per step. XRD studies on the nanostructures were carried out using a Stoe (Mo) StadiP diffractometer with a Mo X-ray source (Mo tube 50 kV 30 mA), monochromated (Pre-sample Ge (111) monochromator selects $K_{\alpha 1}$ only) and a Dectris Mython 1K silicon strip detector covering 18° 2θ. Samples were run in transmission mode, with the sample under rotation in the X-ray beam. All diffraction patterns obtained were compared with database (ICSD) standards. X-ray photoelectron spectroscopy was conducted on a Thermo Scientific K-alpha spectrometer with monochromated Al Kα radiation, a dual beam charge compensation system and constant pass energy of 50 eV (spot size 400 μm). Survey scans were collected in the binding energy range 0–1200 eV. High-resolution peaks were used for the principal peaks of V (2p), O (1s), and C (1s). Data was fitted using CASA XPS software, with doublet separations of 7.5 eV for V (2p) and 2.1 eV for W (4f).[49] Thermochromic measurements were recorded using UV/Vis spectroscopy with a variable temperature stage on a Perkin Elmer Lambda 950 UV/Vis/NIR Spectrophotometer in diffuse reflectance mode. Heating of samples in the UV/Vis spectrometer was achieved by an aluminium temperature cell controlled by RS cartridge heaters, Eurotherm temperature controllers and k-type thermocouples. A Labsphere reflectance standard was used as a reference for the UV/Vis measurements.

Synthesis of [{$VOCl_2(CH_2(COOEt)_2)$}$_4$][1]

Synthesis of [{$VOCl_2(CH_2(COOEt)_2)$}$_4$] was carried out under nitrogen obtained from BOC Ltd. in anhydrous solvents using standard Schlenk techniques. $VOCl_3$ (2 ml, 21.1 mmol) was added to 30 ml of anhydrous *n*-hexane under an atmosphere of nitrogen using a cannula. Diethyl malonate (0.5 ml, 3.3 mmol) was added dropwise and the mixture stirred under nitrogen for 2 h. An excess of $VOCl_3$ was used to ensure complete malonate complexation. Unreacted $VOCl_3$ was removed along with the *n*-hexane *via* filtration, leaving behind a dark red/black solid precipitate. The precipitate was filtered and washed 3 times with *ca.* 20 ml hexane and dried *in vacuo* to give the target compound **1**, in good yield (0.96 g, 83%). ^{1}H and ^{13}C NMR were carried out on this product under nitrogen. A 5 cm^3 concentrated solution of [**1**] in dichloromethane was made up and layered with 15 ml of *n*-hexane. Small crystals formed over approximately a week. ^{1}H NMR ($CDCl_3$): δ 4.18 (q, 4H, –CH_2), δ 3.35 (s, 2H, –CH_2), δ 1.34 (t, 6H, –CH_3). ^{13}C {^{1}H} NMR ($CDCl_3$): δ 14.2 (CH_3), 55.9 (CH_2), 63.6 (CH_2CH_3), 163 (C=O). All peaks were highly broadened due to the paramagnetic nature of the vanadium species. Elemental analysis calculated for $V_4Cl_8C_{28}O_{20}H_{48}$: C, 28.21; H, 4.06. Found: C, 27.33; H, 3.87. Single crystal XRD of [**1**] gave a crystal structure matching that of the tetrameric complex first synthesised by Sobota *et al.* by addition of diethyl malonate to VCl_4 and subsequent exposure to atmospheric oxygen (CCDC: 1307348).[50]

Deposition of thin films

All films were deposited using AACVD. Compound [**1**] (0.30 g, 0.25 mmol) was dissolved in anhydrous toluene (20 ml) and transferred to a glass bubbler under nitrogen using a cannula. The resulting solution was atomized for 5 minutes to ensure complete solvation of the precursor. An aerosol was generated using a piezoelectric humidifier (Ultrasonic Liquids Atomizer LIQUIFOG®). The depositions were carried out using a carrier gas of 2% O_2 in N_2 at a flow rate of 3 L min^{-1}. The glass substrate was standard float glass of 4 mm thickness with a 50 nm SiO_2 barrier layer, supplied by Pilkington/NSG. A top plate was suspended 0.5 cm above the substrate to ensure a laminar flow. A stream of air was introduced into the baffle *via* a second tube, as a means of introducing oxygen to oxidise a precursor.[51] Depositions were carried out at 540 °C, 550 °C and 560 °C, each taking approximately 30 minutes.

Tungsten doping

Tungsten doping was affected by the addition of tungsten(VI) hexaphenoxide [$W(OPh)_6$] into the precursor solution prior to an AACVD deposition. $W(OPh)_6$ was synthesised using a literature protocol by Cross *et al.*[52] ^{1}H NMR (600 MHz, $CDCl_3$) δ 7.21 (12H, m), 6.88 (16H, H), ^{13}C{^{1}H} NMR (600 MHz, $CDCl_3$): δ 161.94 (O–*C*($CH)_2$), δ 128.87(*C*H, *ortho*), δ 123.52(*C*H, *para*), δ 120.51 (*C*H, *meta*). Elemental analysis calculated for $C_{36}H_{30}O_6W$ (%): C, 58.2; H, 4.05. Found: C, 56.5; H, 3.88.

Synthesis of nanoparticles

Nanoparticle samples were prepared using the thermal decomposition of [**1**] in the presence of a high boiling point solvent and alkyl surfactants. Briefly, compound [**1**] (0.5 g, 0.41 mmol) was weighed out into a nitrogen-purged three-necked 250 ml flask with a condensor. At this stage, 1-octadecene (dried over sodium) (20 ml), oleylamine (Table 1), oleic acid (Table 1) and 1,4-tetradecanediol were added. The flask was subjected to 3 vacuum/back fill cycles with nitrogen and heated to the required synthesis temperature (Table 1) at a heating rate of 3.3 °C min^{-1} under dynamic nitrogen. Once the desired temperature was reached, the temperature was maintained for 1 hour before cooling to room temperature naturally. The reaction remained under nitrogen throughout the cooling period. The nanoparticles were precipitated with ethanol (*ca.* 100 ml) and centrifuged at 3000 × *g*. The precipitate was subjected to three further ethanol washes (3 × 100 ml)/centrifugation cycles before storage in a vacuum desiccator. Due to the presence of the alkyl

Table 1 Summary and sample monikers of nanocrystals obtained from the decomposition of [{$VOCl_2(CH_2(COOEt)_2)$}$_4$]

Sample number	Synthesis temperature/°C	Oleylamine/ mmol	Oleic acid/ mmol
1	320	6	6
2	320	9	3
3	320	3	9
4	320	0	12
5	320	12	0
6	280	6	6
7[a]	240	6	6
8[b]	320	6	6

[a] No reaction, non-colloidal blue solution formed. [b] Addition of 1,4-tetradecanediol.

surfactants, the nanomaterials exhibited a high level of dispersibility in organic solvents such as chloroform and *n*-hexane.

Annealing

Nanoparticle samples were annealed in a tube furnace under a constant argon flow of 0.6 L min^{-1} for 10 hours at 550 °C at a heating rate of 10 °C min^{-1} and allowed to cool to room temperature naturally under argon flow before analysis.

Results and discussion

1. Precursor synthesis

$[\{VOCl_2(CH_2(COOEt)_2)\}_4]$ [**1**], was synthesised under an atmosphere of nitrogen as per literature procedure.[53] It is widely reported that the Achilles heel of vanadium(v) precursors for the formation of VO_2 is the 5+ oxidation state (these precursors preferring the formation of V_2O_5) and as such vanadium(IV) precursors were sought for this work. Recently our group reported a synthetic study on the reactivity of vanadium(v) oxytrichloride with a range of ligands in order to isolate and fully characterise a library of novel vanadium precursors.[53] Interestingly, striking ligand dependant structural and chemical variations were exhibited, altering the functionality of these compounds. This recent work described the reaction of vanadium(v) oxytrichloride with the smaller β-diketonate: acetylacetonate (acac) which resulted in the formation of HCl and a vanadium(v) monomeric species. Additionally, reaction with the larger diethyl succinate ligand was reported to proceed with elimination of Cl_2 and reduction of the vanadium centre, which yielded the more reactive (although polymeric) vanadium(IV) species. It was shown that the use of a ligand slightly smaller than the succinate: diethyl malonate, prevented the unwanted polymerisation, whilst still reducing the vanadium(v) oxytrichloride to vanadium(IV) which was desirable, forming the tetrameric precursor: $[\{VOCl_2(CH_2(COOEt)_2)\}_4]$.

Since the reaction of vanadium(v) oxytrichloride with diethyl malonate does not chemically alter the ligand, and instead, it coordinates *via* both carbonyl oxygen atoms to the vanadium centre, we propose that this coordination then facilitates a bond between V and a Cl atom to break, thus reducing the metal centre. Four of these units then come together, the vanadium(IV) centre being stabilised through the coordinating V=O from another identical unit, resulting in the tetramer shown below (Scheme 1). This mechanism is confirmed through spectroscopic analysis: of particular interest the ^{1}H NMR which indicates no loss of proton from the diethylmalonate backbone as well as the longer C–O bond lengths reported in the single crystal X-ray structure, 1.492(7) and 1.498(7) Å (compared with 1.398(4) Å and 1.383(4) in the $[VOCl_2(acac)]$ compound).[53]

2. Film deposition

All films were deposited using AACVD. This differs from traditional CVD insofar as AACVD involves delivery of the precursor to the substrate in the liquid phase at room temperature rather than the deposition of films from high temperature vapours, requiring volatile precursors. In AACVD, the precursor is dissolved in a suitable solvent, from which an aerosol is generated. The precursor-containing aerosol droplets are transported into the reaction vessel *via* a carrier gas, at which point the high temperature inside the reactor causes the solvent to evaporate bringing the precursor in contact with the substrate. The precursor then undergoes decomposition, nucleation and crystal growth to form a thin film. As the transport of the precursor to the substrate is a liquid phase process, the volatility of the precursor becomes unimportant, the suitability of the precursor instead being dependant on its solubility in a suitable solvent system. This enables a range of new precursor molecules to be employed. Additionally, the cost and complexity of the delivery process is reduced considerably, thus making AACVD suitable for industrial scale-up.

In all depositions, toluene was used as the solvent. The precursor for both the VO_2 film and the tungsten dopant were both dissolved in the same solution and transported to the reactor using a carrier gas consisting of 98% nitrogen and 2% oxygen. It is noteworthy that in order to attain VO_2 (M), a separate oxygen source was required in order to counteract the reducing nature of an almost total azotic atmosphere. Due to the air sensitive nature of [**1**], a dual stream of air and nitrogen would be highly detrimental as the precursor would oxidise before entering the reaction chamber. Therefore, a separate gas stream has to be introduced into the chamber itself. This is shown in the schematic in Scheme S1 (ESI†).

Thin films of VO_2 were deposited *via* AACVD of [**1**] in toluene over a temperature range of 540–560 °C using a carrier gas of 2% O_2 in N_2 at a flow rate of 3 L min^{-1} in order to encourage

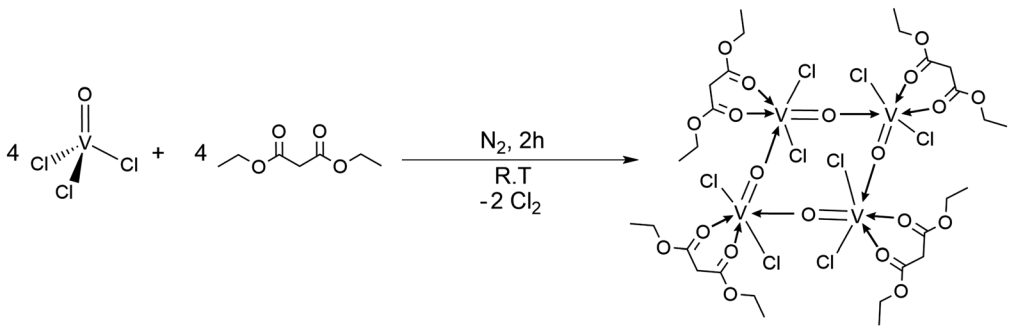

Scheme 1 Synthesis of $[\{VOCl_2(CH_2(COOEt)_2)\}_4]$, designated compound [**1**].

oxidation of the precursor. The deposited films were of good coverage and pale yellow in colour, with some darker, metallic patches formed at higher temperatures. It is noteworthy that AACVD of films at 500 °C did not deposit, whilst raising the temperature to 600 °C yielded poorly crystalline films (see Fig. S4 and S5, ESI†).

Tungsten was doped into the films over a range of concentrations from (0.4–0.8%) by adding small amounts of tungsten(VI) hexaphenoxide [$W(OPh)_6$] to the precursor solution. [$W(OPh)_6$] was chosen as the tungsten source as it is better suited to lower temperature applications due to its ease of handling in air and good solubility in the chosen AACVD solvent (toluene) when compared to other tungsten sources such and WF_6 and WCl_6. The molecular mass of [$W(OPh)_6$] as a percentage of [**1**] present in the precursor solution ranged from 5% to 1%. The W doped films each had greater optical transparency than the undoped films deposited at the same temperature, with colours ranging from pale yellow to azure, becoming more blue with increased concentration. All films were fairly adherent, resisting the "Scotch Tape" test.[54,55]

SEM images were obtained for films of VO_2 deposited at 550 °C, both with and without the incorporation of tungsten into VO_2 film. The undoped film consisted of highly disordered rod-like parties of width approximately 50 nm and length 300–500 nm (Fig. 1a). Incorporation of tungsten into the film appears to greatly alter the morphology, with the film consisting of densely packed, rounded, vertical protrusions with a width of around 100 nm, typical of doped VO_2 thin films obtained by CVD (Fig. 1b).[11,26,29]

XRD patterns were referenced against those of VO_2 (M) (ICSD: 34033), VO_2 (A) (ICSD: 51213), VO_2 (B) (ICSD: 199) V_2O_5 (ICSD: 15798) and V_2O_3 (ICSD: 1473). Films deposited in the temperature range 540–560 °C were indexed as VO_2 (M) as seen in Fig. 1c. There were, however, additional peaks in the XRD patterns, which indicated low levels of an impurity phase, such as a Magneli.[56] There was no evidence of either V_2O_3 or V_2O_5 in the XRD patterns. Tungsten incorporation induces a slight shift in the XRD pattern (27.8° (011) for undoped VO_2 *versus* 27.9° (011) for W-doped) and a loss of crystallinity. This, coupled with the lowering of the MST is highly indicative of successful doping. Film thickness, measured by side-on SEM (see Fig. S7, ESI†), gave increasing thicknesses ranging between 1.8 ± 0.2 μm for the VO_2 grown at 540 °C, 2.1 ± 0.6 μm for 550 °C and 4.1 ± 1.6 μm for 560 °C. Tungsten doping at the same temperatures gave thicker films with W–VO_2 grown at 550 °C giving a thickness of 2.8 ± 0.5 μm.

Typical XPS data from VO_2 (M) and W-doped VO_2 (M) thin films are shown in Fig. 2. The V2p spectra are split into two regions which were then fitted with two separate environments as it was clear that more than one oxidation state was present. The visible shoulders of the main $V2p_{3/2}$ peak indicate the presence of $V^{(IV)}$ in the films. XPS is highly surface sensitive, and as such a higher proportion of V_2O_5 was present at the surface than in the film, hence a large $V^{(V)}$ peak. Surface vanadium species will always be oxidised and this is commonly observed for XPS spectra of thin films of VO_2.[57,58] The fitted

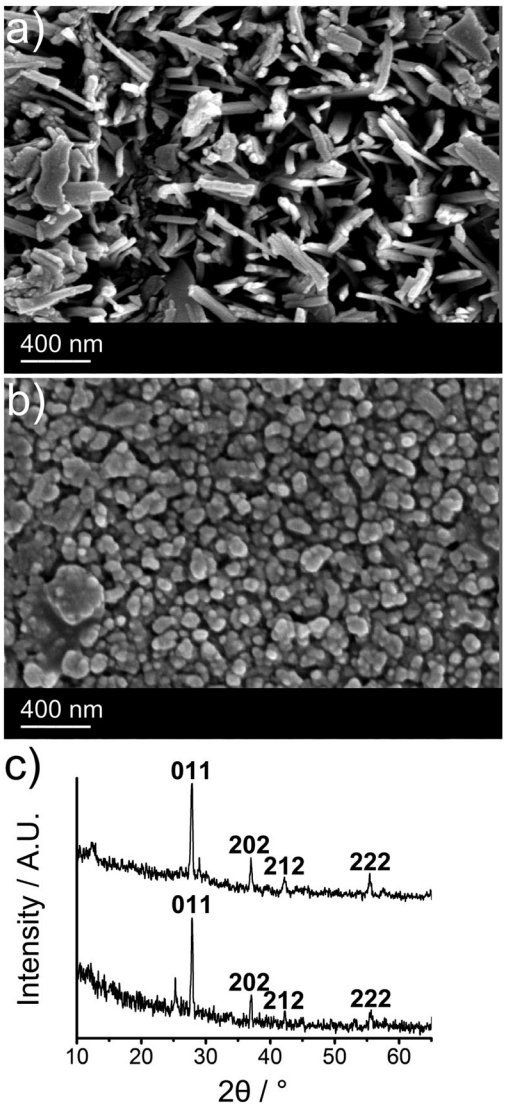

Fig. 1 SEM images of the VO_2 film deposited from [**1**] in toluene at (a) 550 °C using a 2% O_2 in N_2 carrier gas, and (b) the film W doped VO_2 film deposited from [**1**] with 5 at% $W(OPh)_6$ in toluene at 550 °C using N_2 carrier gas. (c) Shows XRD patterns for a VO_2 (M) film deposited at 550 °C (c) (top) and a W-doped VO_2 (M) film also deposited at 550 °C (c) (bottom).

peak positions of 516.5 eV and 516.7 eV for $V2p_{3/2}$ in the undoped and doped films respectively are indicative of $V^{(IV)}$ in VO_2.[49] The second feature at higher binding energy in both spectra (518.1 eV and 518.2 eV respectively) was assigned to V_2O_5.[49]

The W 4f environment showed the presence of only one oxidation state. This gave a value of 35.28 eV (W $4f_{7/2}$) and 37.38 eV (W $4f_{5/2}$) which is consistent with W^{6+}. This has been previously seen for W-doped VO_2 in both thin film and nanoparticle synthesis.[1,29,59]

Variable temperature transmission UV/Vis spectroscopy was carried out on the films deposited from [**1**] in order to determine whether the films underwent the structural transition associated with VO_2 (M). A spectrum was taken of the film at room temperature. Following this the films were rapidly heated

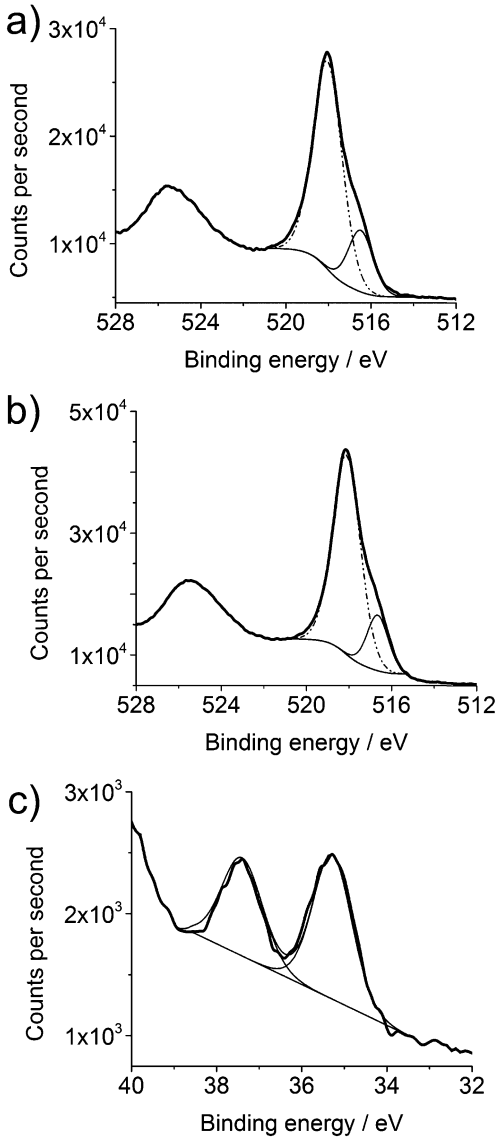

Fig. 2 Detailed XPS scans of: (a) V2p$_{3/2}$ of a VO_2 (M) thin film formed from the AACVD of [{$VOCl_2(CH_2(COOEt)_2)$}$_4$] [**1**] at 550 °C (showing $V^{(IV)}$ at lower binding energy (thin solid line) *vs.* $V^{(V)}$ (dotted line)), (b) V2p$_{3/2}$ of a W-doped VO_2 (M) thin film at 550 °C and (c) corresponding W 4f scan.

to 90 °C and the measurement repeated. The films were then cooled to room temperature and the initial measurement repeated to ensure that the sample has remained in the same position throughout the heating (Fig. 3).

Films deposited at 550 °C showed the highest MST by a considerable margin, with the transmittance at 2500 nm falling from 60% to around 2% when the sample was heated from room temperature to 90 °C. Films deposited at 560 °C demonstrated similar characteristics at room temperature to those deposited at 550 °C. Testing the samples for thermochromic activity revealed that the monoclinic phase of the VO_2 is far less pure, roughly halving the transmission to 30%. The VO_2 film deposited at 540 °C was by far the least effective, seeing a reduction in transmission from 50% to 40% at 2500 nm. These measurements reveal that the optimum temperature for the formation of monoclinic VO_2 from [**1**] was 550 °C. All undoped films displayed a phase transition temperature of *ca.* 68 °C, which is typical of undoped VO_2 (M).[60] Tungsten doped films exhibited a reduction in MST, to *ca.* 50 °C. This was determined from hysteresis data obtained *via* UV/Vis spectroscopy, giving a narrow temperature window for the transition of *ca.* 5 °C (see Fig. S6, ESI†).

Solar modulation calculations (ΔT_{sol}) were performed as described by Taylor *et al.*[61] Solar modulation values take into account the effect that gases, such as CO_2 and H_2O, have on the intensity of solar radiation at ground level. This gives a value which can be used to give a better representation of the absolute change in the optical properties of the material. The majority of the energy in the solar spectrum, at ground level, is accounted for by the UV/Visible region (380–780 nm); this leaves a maximum change of *ca.* 20% for the near IR region (780–2500 nm). VO_2 (M) shows negligible changes in visible wavelength absorption/transmission when it passes through the MST. When comparing the solar modulation values for the VO_2 films, it can be seen that the sample deposited at 550 °C shows a solar modulation of 15.9% which is close to this maximum allowed solar modulation for single layer VO_2 (M) and is comparable to the best results seen for VO_2 thin films by other research groups.[60]

3. Nanostructure synthesis and characterisation

Nanostructures were also synthesised from [{$VOCl_2(CH_2(COOEt)_2)$}$_4$] [**1**] using thermal decomposition in the presence of a high boiling point solvent and structure-directing surfactants under an inert atmosphere. Thermal decomposition of metal–organic precursors has been shown to be extremely effective at producing nanoparticles with low polydispersity and shape anisotropy which are subsequently dispersible in a wide range of [organic] solvents.[62–65] A large number of the metal oxide nanoparticle syntheses are based on the *in* or *ex situ* formation of metal–fatty acid complexes and their subsequent decomposition to yield the metal oxide nanoparticles forested by surfactants (fatty acids) rendering them readily dispersible in organic solvents.[66–70]

Examples using this methodology for VO_2 nanocrystals are few and far between, however it is noteworthy that Paik *et al.* utilised a similar methodology to synthesise VO_x nanocrystals from $VOCl_3$ in the presence of oleylamine and octadecanol, resulting in colloidally stable, monodisperse mixed-phase VO_x nanocrystals.[71] The VO_x nanocrystals obtained were flash-annealed at 500 °C for 5 minutes in air at 1 mTorr in order to give thermochromic VO_2 (M), as the formation of phase-pure VO_2 (M) at low (<450 °C) temperature and atmospheric pressure is thermodynamically unfavourable.[18] The authors make reference to the fact that no reaction occurs from $VOCl_3$ without 1-octadecanol as vanadium–oxygen bonds are formed from the non-hydrolitic reaction between a primary alcohol and a metal halide (*sic* 1-octadecanol and $VOCl_3$).[71–73] Although the synthesis described herein is conspicuous by the absence of a primary alcohol, the composition of the precursor with co-ordinated oxygen species is the *de facto* product of the non-hydrolitic reaction described above. This, coupled with the high temperature of the synthesis,

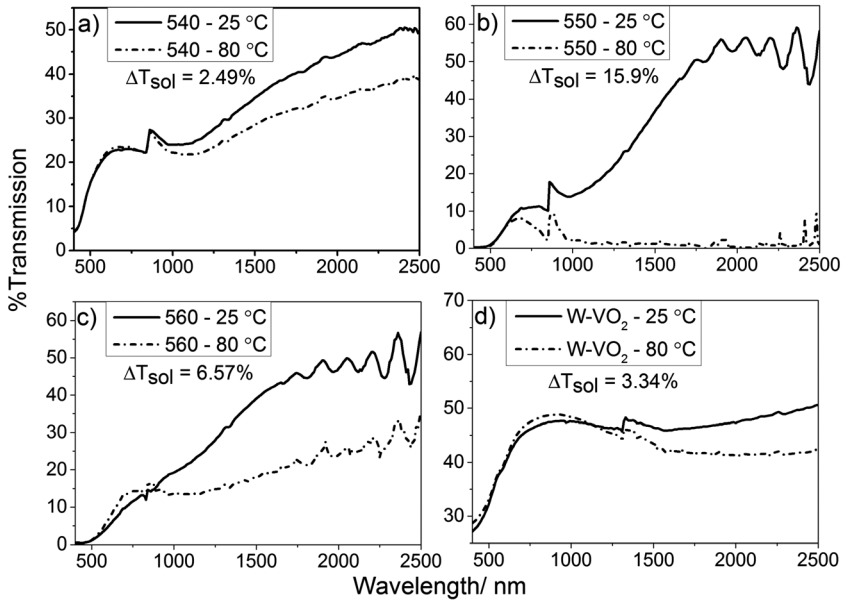

Fig. 3 Variable temperature UV/Vis/NIR spectra showing the change in optical properties of thin films of undoped and W-doped VO_2 thin films deposited by AACVD of synthesised vanadium precursor solutions. Solar modulation values (ΔT_{sol}) for each film have been included in the figure. (a) VO_2 (M) film deposited at 540 °C, (b) 550 °C, (c) 560 °C and (d) W-doped VO_2 (M) thin film deposited at 550 °C.

allows the nucleation and growth of VO_x nanoparticles to proceed.

The investigation on the decomposition of [**1**] in the presence of surfactants in a high boiling point solvent was designed to investigate the effect of differing surfactant ratios, temperature and the inclusion of a fatty alcohol, 1,4-tetradecanediol. The sample preparation conditions are summarised in Table 1. All reactions were undertaken in 20 ml of dry 1-octadecene (dried over sodium) and after 3 vacuum/re-fill cycles of nitrogen. The reaction was heated from room temperature to the target temperature at 3.3 °C min^{-1} under a dynamic flow of nitrogen, during which the reaction mixture darkened in colour from green to a final black. The addition of oleylamine also induced a colour change of the precursor to blue, presumably due to complexation with the vanadium centre, most likely a d → d transition due to the formation of an octahedral complex. On precipitation with ethanol and centrifugation all samples (bar sample 7) gave a black precipitate which could be readily dispersed in organic solvents.

From TEM analysis of the different samples, it was clear that different surfactant blends affected the morphology of the final product. Oleylamine in particular promoted the growth of spine-like structures as well as nanoparticles which were not seen in its absence, whereas oleic acid purely promoted particle growth. Mixtures of oleic acid and oleylamine were found to be the most effective at generating readily dispersible products, with the optimum blend of equimolar amounts of oleic acid and oleylamine [used by Sun and Zeng in their seminal paper on iron oxide nanoparticle synthesis][74] in samples 1, 6, 7 and 8. The "6,6" blend produced a mixture of some small particles but predominantly large, spine-like structures of 50–100 nm in length. These features were preserved on annealing in nitrogen for 8 hours, but were not as pronounced in sample 6, in which the synthesis temperature is lower (280 °C), leading us to deduce that the formation of the vanadium oxide spines is temperature as well as oleylamine dependent. However, the features emerged with annealing treatment at 550 °C under nitrogen for 10 hours (Fig. 4d and e). Sample 7, in which the synthesis temperature was reduced to 240 °C was evidently lower than the nucleation temperature for this system as no nanoparticles were produced. The addition of an oxygen source, 1,4-tetradecanediol in sample 9 with the "6,6" blend of oleic acid and oleylamine had no effect on the phase and seemed to the 1,4-tetradecanediol counteracted the structure-directing effects of oleylamine to form almost exclusively particulate material (Fig. S2d, ESI†).

Detailed TEM analysis of the as-synthesised VO_x nanostructures (especially lattice plane images) were exacting due to the presence of high carbon contamination, predominantly caused by surfactant layers and decomposition products from the precursor itself. The latter was in evidence through the presence of chlorine by EDS as residue from initial $VOCl_3$ (Fig. 4c and f).

Samples 1 and 6 were both annealed at 550 °C under argon in order to increase crystallinity. Analysis of lattice planes in the annealed samples (Fig. 4e) gave a *d*-spacing of 0.326 nm corresponding to the ⟨111⟩ plane of vanadium oxide (V_4O_9, ICSD 15041). Analysis of lattice planes in Fig. S3 (ESI†) gave a *d*-spacing of 0.327 nm, again corresponding to the ⟨111⟩ plane of V_4O_9, confirming that heat treatment had an identical effect on both samples despite initial differences with synthesis temperatures.

EDS spectra showed the persistence of chlorine in the system as a consequence of the chlorine in the precursor. It also showed

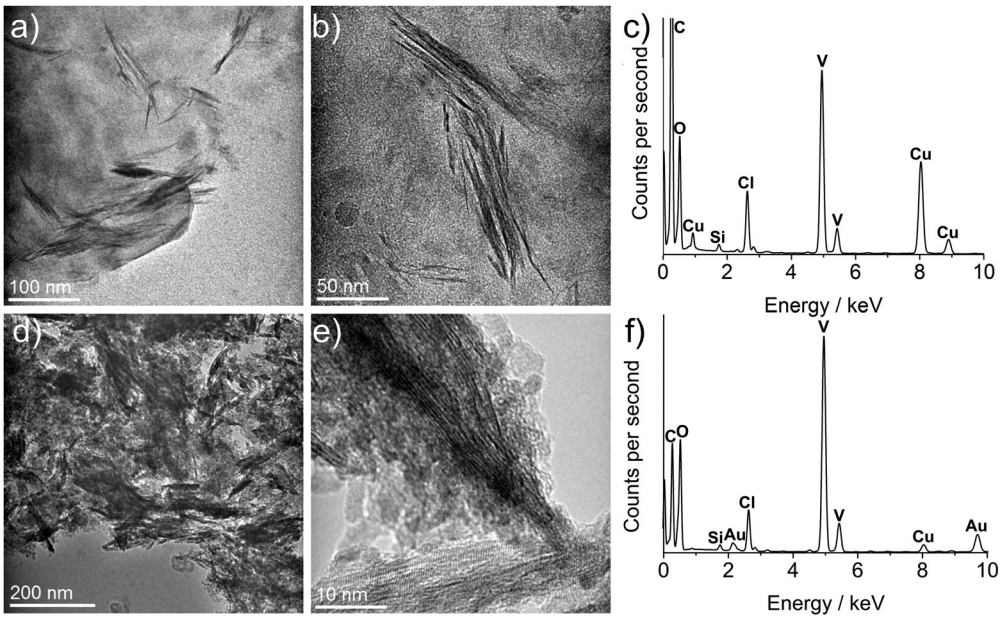

Fig. 4 TEM images and EDS spectra of sample 1 pre- and post annealing. (a and b) are TEM images of pre-annealed sample 1, showing the directing effects of oleylamine and the formation of a spine-like morphology. (c) is the corresponding EDS spectrum of the pre-annealed sample 1. (d and e) are annealed TEM images from sample 1 with corresponding EDS spectrum, (f).

the reduction in carbon from the heavily carbon contaminated pre-annealed samples *versus* post annealed samples, attributed to the alkyl ligands. The at% ratios of V : O for samples 1 and 6 pre-anneal was 26.20 : 73.80 and 1.91 : 98.09 respectively, with heat treatment dramatically effecting sample 6 with the ratio changing to 26.22 : 73.78. The ratio for sample 1 however, was relatively unchanged (26.40 : 73.60). These non-stoichiometric amounts, along with HRTEM and XRD analysis, leads us to conclude that a mixture of vanadium oxide phases were formed in the nanoparticle synthesis. Ratios of V : O for all samples are listed in the Table S1 (ESI†).

Powder X-ray diffraction (PXRD) was performed on the as synthesised and the post-annealed nanoparticle samples as shown in Fig. 5. The as-synthesised nanoparticles, Fig. 5a and b,

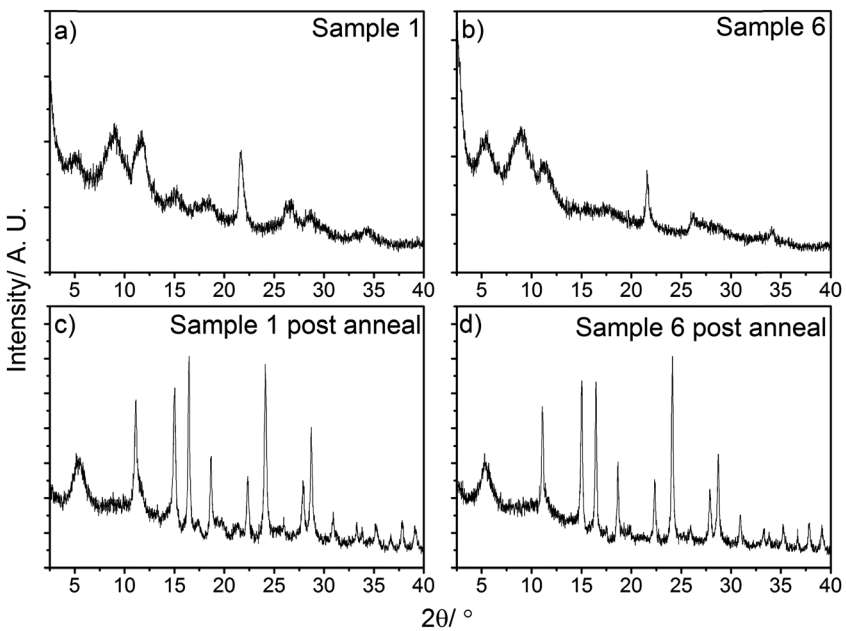

Fig. 5 PXRD diffraction patterns for as synthesised powders, (a) and (b) and following annealing treatment, (c) and (d). λ = 0.7093 Å. Sample 1 and 6 were synthesised from the decomposition of $[\{VOCl_2(CH_2(COOEt)_2)\}_4]$ in the presence of oleic acid (6 mmol) and oleylamine (6 mmol) at 320 °C (Sample 1) and 280 °C (Sample 6).

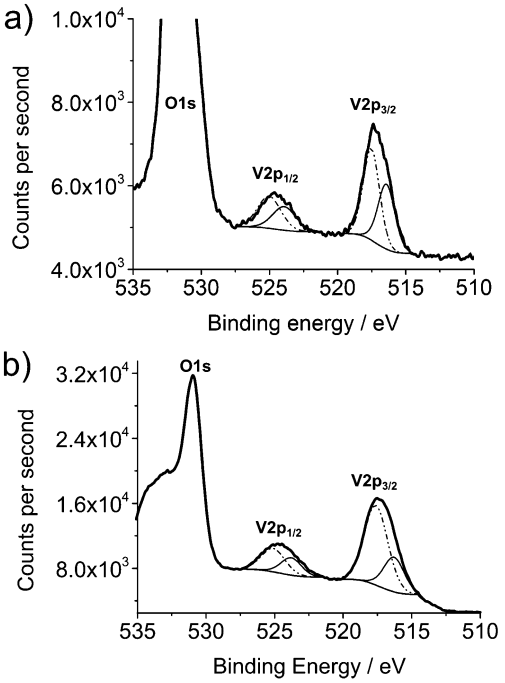

Fig. 6 Detailed XPS scans of: (a) V2p of sample 1, VO_2 nanomaterials before annealing and (b) after annealing showing $V^{(IV)}$ at lower binding energy (thin solid line) *vs.* $V^{(V)}$ (dotted line).

have only a few diffraction peaks- it was not possible to confirm the phase of the material from these. The broad reflections between 5–12° 2θ also suggest that there was a large amorphous component to the samples.

The post-annealed samples, Fig. 5c and d, have a greater number of diffraction peaks in the data. The intensities of these diffraction peaks are also greater, with a reduction in the number of broad diffraction peaks-suggesting higher crystallinity for the annealed samples. Phase analysis of these samples suggested a mix of Magneli phases, with V_3O_7 – 22.2° ⟨020⟩, V_4O_9 – 11.1° ⟨102⟩, 16.5° ⟨113⟩ and V_5O_9 – 5.2° ⟨001⟩, 24.1° ⟨211⟩ and 28.8° ⟨203⟩ lattice planes all being identified in the data. This is not surprising, as vanadium is known to readily form oxides with multiple oxidation states of vanadium present.[75,76]

XPS was used as a comparison between annealed and non-annealed samples. XPS spectra for the V2p region in Sample 1 pre (a) and post (b) anneal are shown in Fig. 6. Both show similar profiles to the thin films in Fig. 2, with $V^{(IV)}$ peaks reported at 516.5 eV and 516.3 eV for non-annealed and annealed samples respectively ($V2p_{3/2}$) and assigned as VO_2. The $V^{(V)}$ peaks, at 517.7 eV and 517.8 eV respectively were again assigned as V_2O_5.[49]

Conclusions

The synthesis of [{$VOCl_2(CH_2(COOEt)_2)$}$_4$] [**1**] was demonstrated, and its versatility as an AACVD precursor for vanadium oxide thin films and nanocrystals investigated. [**1**] was shown to be a highly effective precursor for the formation of thermochromic VO_2 (M) thin films on glass by AACVD. The AACVD process has numerous advantages over conventional CVD methods including: the wide range of precursors including those with low volatility, high control over dopant concentration and is applicable to industrial scale-up.[6] VO_2 (M) films produced at 550 °C (ΔT_{sol} = 15.9%) were shown to have superior solar modulation when compared to films produced at 540 °C and 560 °C and compare favourably with literature values. The thermochromic switching temperature was reduced through the addition of [$W(OPh)_6$] to the precursor solution, reducing the MST to ~50 °C. This demonstrates the viability of the AACVD method when using a designed molecular precursor to form thermochromic materials with tunable properties.

In terms of nanomaterial synthesis, [**1**] was decomposed in the presence of alkyl surfactants at elevated temperatures in an inert atmosphere. It was shown that different surfactants affected the shape of the final product, with oleylamine promoting "spine-like" growth, and oleic acid particulate material. The control over shape and size of the resultant nanomaterials by manipulation of surfactant type and concentration in the decomposition of [**1**] bodes well for the future for designed molecular vanadium oxide nanomaterial precursors. [**1**] represents the first example in a class of activated vanadium complexes for the synthesis of a variety of VO_2 thin films and shape tunable V_xO_y nanomaterials. The design of these molecules may lead to a single precursor for the low temperature, one-pot synthesis of colourless thermochromic VO_2 (M) nanocrystals – a key step towards the routine use of smart windows, potentially saving millions of kWh per annum worldwide.

Acknowledgements

JCB and CEK acknowledge the Ramsay Memorial Trust for funding by means of Ramsay Memorial Fellowships. BB acknowledges Huntsman Pigments and the Energy and Physical Research Council (EPSRC) for an EngD studentship (Grant No. EP/G036675). IPP, CJC and MJP acknowledge EPSRC Grant No. EP/L017709 for funding.

References

1 M. E. A. Warwick and R. Binions, *J. Mater. Chem. A*, 2014, **2**, 3275.
2 C. G. Granqvist, *J. Vac. Sci. Technol., B*, 2014, **32**, 60801.
3 M. Kamalisarvestani, R. Saidur, S. Mekhilef and F. S. Javadi, *Renewable Sustainable Energy Rev.*, 2013, **26**, 353–364.
4 C. G. Granqvist, *Sol. Energy Mater. Sol. Cells*, 2007, **91**, 1529–1598.
5 P. Huovila, *Buildings and Climate Change: Status, Challenges, and Opportunities*, UNEP/Earthprint, 2007.
6 P. Marchand, I. A. Hassan, I. P. Parkin and C. J. Carmalt, *Dalton Trans.*, 2013, **42**, 9406–9422.
7 S. M. Babulanam, T. S. Eriksson, G. A. Niklasson and C. G. Granqvist, *Sol. Energy Mater.*, 1987, **16**, 347–363.
8 J. B. Goodenough, *Annu. Rev. Mater. Sci.*, 1971, **1**, 101–138.

9 M. Saeli, C. Piccirillo, I. P. Parkin, R. Binions and I. Ridley, *Energy Build.*, 2010, **42**, 1666–1673.
10 C. Batista, R. M. Ribeiro and V. Teixeira, *Nanoscale Res. Lett.*, 2011, **6**, 1–7.
11 C. Piccirillo, R. Binions and I. P. Parkin, *Thin Solid Films*, 2008, **516**, 1992–1997.
12 G. V. Jorgenson and J. C. Lee, *Sol. Energy Mater.*, 1986, **14**, 205–214.
13 W. Burkhardt, T. Christmann, S. Franke, W. Kriegseis, D. Meister, B. K. Meyer, W. Niessner, D. Schalch and A. Scharmann, *Thin Solid Films*, 2002, **402**, 226–231.
14 S. Hu, S.-Y. Li, R. Ahuja, C. G. Granqvist, K. Hermansson, G. A. Niklasson and R. H. Scheicher, *Appl. Phys. Lett.*, 2012, **101**, 201902.
15 T. J. Hanlon, J. A. Coath and M. A. Richardson, *Thin Solid Films*, 2003, **436**, 269–272.
16 X. Tan, T. Yao, R. Long, Z. Sun, Y. Feng, H. Cheng, X. Yuan, W. Zhang, Q. Liu, C. Wu, Y. Xie and S. Wei, *Sci. Rep.*, 2012, **2**, 466.
17 R. Long, B. Qu, R. Tan, Y. Sun, X. Tan, W. Ying, B. Pan, Y. Xiong and Y. Xie, *Phys. Chem. Chem. Phys.*, 2012, **14**, 7225–7228.
18 C. H. Griffiths and H. K. Eastwood, *J. Appl. Phys.*, 1974, **45**, 2201–2206.
19 M. Borek, F. Qian, V. Nagabushnam and R. K. Singh, *Appl. Phys. Lett.*, 1993, **63**, 3288–3290.
20 N. R. Mlyuka, G. A. Niklasson and C. G. Granqvist, *Sol. Energy Mater. Sol. Cells*, 2009, **93**, 1685–1687.
21 T. D. Manning, I. P. Parkin, C. Blackman and U. Qureshi, *J. Mater. Chem.*, 2005, **15**, 4560–4566.
22 M. N. Field and I. P. Parkin, *J. Mater. Chem.*, 2000, **10**, 1863–1866.
23 U. Qureshi, T. D. Manning and I. P. Parkin, *J. Mater. Chem.*, 2004, **14**, 1190–1194.
24 M. B. Sahana, M. S. Dharmaprakash and S. A. Shivashankar, *J. Mater. Chem.*, 2002, **12**, 333–338.
25 T. D. Manning and I. P. Parkin, *Polyhedron*, 2004, **23**, 3087–3095.
26 T. D. Manning and I. P. Parkin, *J. Mater. Chem.*, 2004, **14**, 2554–2559.
27 T. D. Manning, I. P. Parkin, R. J. H. Clark, D. Sheel, M. E. Pemble and D. Vernadou, *J. Mater. Chem.*, 2002, **12**, 2936–2939.
28 D. Vernardou, P. Paterakis, H. Drosos, E. Spanakis, I. M. Povey, M. E. Pemble, E. Koudoumas and N. Katsarakis, *Sol. Energy Mater. Sol. Cells*, 2011, **95**, 2842–2847.
29 C. S. Blackman, C. Piccirillo, R. Binions and I. P. Parkin, *Thin Solid Films*, 2009, **517**, 4565–4570.
30 R. Binions, G. Hyett, C. Piccirillo and I. P. Parkin, *J. Mater. Chem.*, 2007, **17**, 4652–4660.
31 C. Piccirillo, R. Binions and I. P. Parkin, *Eur. J. Inorg. Chem.*, 2007, 4050–4055.
32 M. E. A. Warwick, I. Ridley and R. Binions, *J. Nanosci. Nanotechnol.*, 2011, **11**, 8158–8162.
33 S. S. Garje, J. S. Ritch, D. J. Eisler, M. Afzaal, P. O'Brien and T. Chivers, *J. Mater. Chem.*, 2006, **16**, 966–969.
34 N. O. Boadi, M. A. Malik, P. O'Brien and J. A. M. Awudza, *Dalton Trans.*, 2012, **41**, 10497–10506.
35 J. M. Clark, G. Kociok-Köhn, N. J. Harnett, M. S. Hill, R. Hill, K. C. Molloy, H. Saponia, D. Stanton and A. Sudlow, *Dalton Trans.*, 2011, **40**, 6893–6900.
36 M. J. Powell, P. Marchand, C. J. Denis, J. C. Bear, J. A. Darr and I. P. Parkin, *Nanoscale*, 2015, **7**, 18686–18693.
37 T.-D. Nguyen and T.-O. Do, *Langmuir*, 2009, **25**, 5322–5332.
38 J.-H. Son, J. Wei, D. Cobden, G. Cao and Y. Xia, *Chem. Mater.*, 2010, **22**, 3043–3050.
39 H. Zhang, X. Xiao, X. Lu, G. Chai, Y. Sun, Y. Zhan and G. Xu, *J. Alloys Compd.*, 2015, **636**, 106–112.
40 J. Nag and R. F. Haglund Jr., *J. Phys.: Condens. Matter*, 2008, **20**, 264016.
41 L. Zhong, M. Li, H. Wang, Y. Luo, J. Pan and G. Li, *CrystEngComm*, 2015, **17**, 5614–5619.
42 P. Billik, M. Čaplovičová, J. Maňka, Ľ. Čaplovič, A. Cigáň, A. Koňakovský, R. Bystrický and A. Dvurečenskij, *Meas. Sci. Technol.*, 2011, **11**, 29–33.
43 K. C. Kam and A. K. Cheetham, *Mater. Res. Bull.*, 2006, **41**, 1015–1021.
44 Y. Zhang, J. Zhang, X. Zhang, Y. Deng, Y. Zhong, C. Huang, X. Liu, X. Liu and S. Mo, *Ceram. Int.*, 2013, **39**, 8363–8376.
45 B.-G. Chae, H.-T. Kim, S.-J. Yun, B.-J. Kim, Y.-W. Lee, D.-H. Youn and K.-Y. Kang, *Electrochem. Solid-State Lett.*, 2006, **9**, C12–C14.
46 H. Wang, X. Yi, S. Chen and X. Fu, *Sens. Actuators, A*, 2005, **122**, 108–112.
47 S. A. Pauli, R. Herger, P. R. Willmott, E. U. Donev, J. Y. Suh and R. F. Haglund Jr, *J. Appl. Phys.*, 2007, **102**, 73527.
48 A. B. Pangborn, M. A. Giardello, R. H. Grubbs, R. K. Rosen and F. J. Timmers, *Organometallics*, 1996, **15**, 1518–1520.
49 NIST X-Ray Photoelectron Spectrosc. XPS Database Version 35.
50 P. Sobota, J. Ejfler, S. Szafert, T. Glowiak, I. O. Fritzky and K. Szczegot, *J. Chem. Soc., Dalton Trans.*, 1995, 1727–1732.
51 N. Noor and I. P. Parkin, *J. Mater. Chem. C*, 2013, **1**, 984–996.
52 W. B. Cross, I. P. Parkin, S. A. O'Neill, P. A. Williams, M. F. Mahon and K. C. Molloy, *Chem. Mater.*, 2003, **15**, 2786–2796.
53 B. J. Blackburn, J. H. Crane, C. E. Knapp, M. J. Powell, P. Marchand, D. Pugh, J. C. Bear, I. P. Parkin and C. J. Carmalt, *Mater. Des.*, 2016, **108**, 780–790.
54 A. Mills, N. Elliott, I. P. Parkin, S. A. O'Neill and R. J. Clark, *J. Photochem. Photobiol., A*, 2002, **151**, 171–179.
55 J. G. Buijnsters, P. Shankar, W. Fleischer, W. J. P. van Enckevort, J. J. Schermer and J. J. ter Meulen, *Diamond Relat. Mater.*, 2002, **11**, 536–544.
56 U. Schwingenschlögl and V. Eyert, *Ann. Phys.*, 2004, **13**, 475–510.
57 R. Quesada-Cabrera, M. J. Powell, P. Marchand, C. J. Denis, F. D. Maggio, J. A. Darr and I. P. Parkin, *J. Nanosci. Nanotechnol.*, 2016, **16**, 10104–10111.
58 S. Lu, L. Hou and F. Gan, *J. Mater. Sci.*, 1993, **28**, 2169–2177.
59 G. P. Halada and C. R. Clayton, *J. Vac. Sci. Technol., A*, 1993, **11**, 2342–2347.

60 A. Taylor, I. Parkin, N. Noor, C. Tummeltshammer, M. S. Brown and I. Papakonstantinou, *Opt. Express*, 2013, **21**(suppl 5), A750–A764.
61 M. J. Powell, R. Quesada-Cabrera, A. Taylor, D. Teixeira, I. Papakonstantinou, R. G. Palgrave, G. Sankar and I. P. Parkin, *Chem. Mater.*, 2016, **28**, 1369–1376.
62 C. R. Crick, J. C. Bear, P. Southern and I. P. Parkin, *J. Mater. Chem. A*, 2013, **1**, 4336–4344.
63 J. Park, K. An, Y. Hwang, J.-G. Park, H.-J. Noh, J.-Y. Kim, J.-H. Park, N.-M. Hwang and T. Hyeon, *Nat. Mater.*, 2004, **3**, 891–895.
64 M. Lattuada and T. A. Hatton, *Langmuir*, 2007, **23**, 2158–2168.
65 J. C. Bear, N. Hollingsworth, P. D. McNaughter, A. G. Mayes, M. B. Ward, T. Nann, G. Hogarth and I. P. Parkin, *Angew. Chem., Int. Ed.*, 2014, **53**, 1598–1601.
66 L. M. Bronstein, J. E. Atkinson, A. G. Malyutin, F. Kidwai, B. D. Stein, D. G. Morgan, J. M. Perry and J. A. Karty, *Langmuir*, 2011, **27**, 3044–3050.
67 L. M. Bronstein, X. Huang, J. Retrum, A. Schmucker, M. Pink, B. D. Stein and B. Dragnea, *Chem. Mater.*, 2007, **19**, 3624–3632.
68 S. G. Kwon, Y. Piao, J. Park, S. Angappane, Y. Jo, N.-M. Hwang, J.-G. Park and T. Hyeon, *J. Am. Chem. Soc.*, 2007, **129**, 12571–12584.
69 S. G. Kwon and T. Hyeon, *Small*, 2011, **7**, 2685–2702.
70 S. G. Kwon and T. Hyeon, *Acc. Chem. Res.*, 2008, **41**, 1696–1709.
71 T. Paik, S.-H. Hong, E. A. Gaulding, H. Caglayan, T. R. Gordon, N. Engheta, C. R. Kagan and C. B. Murray, *ACS Nano*, 2014, **8**, 797–806.
72 M. Niederberger, *Acc. Chem. Res.*, 2007, **40**, 793–800.
73 M. Niederberger, M. H. Bartl and G. D. Stucky, *J. Am. Chem. Soc.*, 2002, **124**, 13642–13643.
74 S. Sun and H. Zeng, *J. Am. Chem. Soc.*, 2002, **124**, 8204–8205.
75 C. Wu, F. Feng and Y. Xie, *Chem. Soc. Rev.*, 2013, **42**, 5157–5183.
76 M. Demeter, M. Neumann and W. Reichelt, *Surf. Sci.*, 2000, **454–456**, 41–44.